Satellites reveal recent increases in global land surface albedo that moderates global warming

Zhengyang Hou[1], Liqiang Zhang[1], Jingjing Peng[2], Giovanni Forzieri[3], Aolin Jia[4], Zhiqiang Xiao[1], Ying Qu[1], Jintai Lin[5], Duoying Ji[1], Zidong Zhu[1], Xin Yao[1], Shuwen Peng[1], Lanpu Zhao[6], Wenjie Fan[7], Zhaocong Wu[6], Hao Geng[1], Qihao Wang[1], Suhong Liu[1] and Liangpei Zhang[6]

[1]State Key Laboratory of Remote Sensing Science, Faculty of Geographical Science, Beijing Normal University, Beijing, China.

[2]Earth System Science Interdisciplinary Center/ Cooperative Institute for Satellite Earth System Studies (CISESS), University of Maryland, College Park, MD, USA.

[3]Department of Civil and Environmental Engineering, University of Florence, Florence, Italy.

[4]Remote Sensing and Natural Resource Modeling, Department ERIN, Luxembourg Institute of Science and Technology, Belvaux, Luxembourg.

[5]Department of Atmospheric and Oceanic Sciences, School of Physics, Peking University, Beijing, China.

[6]Aerospace Information Research Institute, Henan Academy of Sciences, Beijing, China.

[7]School of Earth and Space Sciences, Peking University, Beijing, China.

The File Includes:

1 Supplementary Texts 1-2

2 Supplementary Figures 1-14

3 Supplementary Tables 1-3

1 Supplementary Texts

1.1 Supplementary Text 1

Significance and fluctuations of albedo changes affected by snow dynamics. The change in albedo of snow-free areas globally shows a significant increasing trend (Fig.1a; Mann–Kendall test; P-value=0.018; Student's t-test in local albedo changes see Fig.S4), typically driven by long-term changes in surface properties such as vegetation and water. Our results indicate that albedo changes in snow-free region are usually less than 0.1 during the past two decades, while albedo often increase by 0.5 after land was covered by snow. Moreover, at larger scales, such as 1°x1° grid cells or globally, albedo interannual fluctuations caused by snow cover change also disrupt the significance of the albedo change trends driven by surface properties. During the period 2001-2020, global snow cover areas exhibited a significant decreasing trend (Fig.1a in the main paper; Mann–Kendall test; P-value = 0.012), and the year 2020 was not an anomalous year for snow cover (the linear regression residuals were less than 1.5 times the standard deviation). Furthermore, the GLMA increase caused by the albedo change in snow-free regions was two times as large as the GLMA decrease (195.3%) caused by snow dynamics during 2001-2020, indicating that the GLMA change during 2001-2020 may represent the general trend in global land surface albedo changes over the past two decades, instead of being mainly explained as the fluctuations caused by snow cover change.

1.2 Supplementary Text 2

Comparisons with previous results. Compared with previous research on albedo-induced radiative forcing caused by anthropogenic changes in land use [1–4], our findings exhibit agreement. Land-use forcing is defined as those changes in land-surface properties directly caused by human activity rather than by climate processes (IPCC AR6). Lejeune et al. [4] and Smith et al. [3] individually quantified land-use radiative forcing using CMIP5 and CMIP6 models; and their results were -0.11±0.09 W/m^2 during 1850-2014 and -0.11 (-0.16 to -0.04) W/m^2 during 1850-2000. The two studies focused on the changes in land use due to shifts in agricultural practices and deforestation leading to primary/secondary forest. Ghimire et al. [2] provided a MODIS/AVHRR-based radiative forcing of approximately -0.12 W/m^2 from 1850, consistent with the results of CMIP5 and CMIP6. They established a one-to-many or one-to-one mapping between the 6 land-use types in Land-use Harmonization (LUH) dataset [5] and the 17 land cover types defined by the International Geosphere-Biosphere Plan (IGBP), and reconstructed LULC conversions at a 500m resolution. The radiative forcing was estimated by combining the reconstructed LULC conversions and an albedo lookup map without albedo interannual variations [6]. Based on the above results, IPCC AR6 estimated land-use radiative forcing of -0.15±0.1 W/m^2 during 1750-2019, excluding the forcing by irrigation at 0.05 W/m^2. The radiative forcing decreased on average by 0.00073 W/m^2/year. We used the Ghimire's mapping method to group the 16 land cover types excluding permanent snow and ice into the 6 LULC types in the LUH dataset (Supplementary Table S3). Conversions between the 6 land-use types from 2001 to 2020 resulted in a radiative forcing of -0.01004 W/m^2, with a reduction of 0.00053 W/m^2/year, slightly lower than 0.00073 W/m^2/year given by IPCC.

2 Supplementary Figures

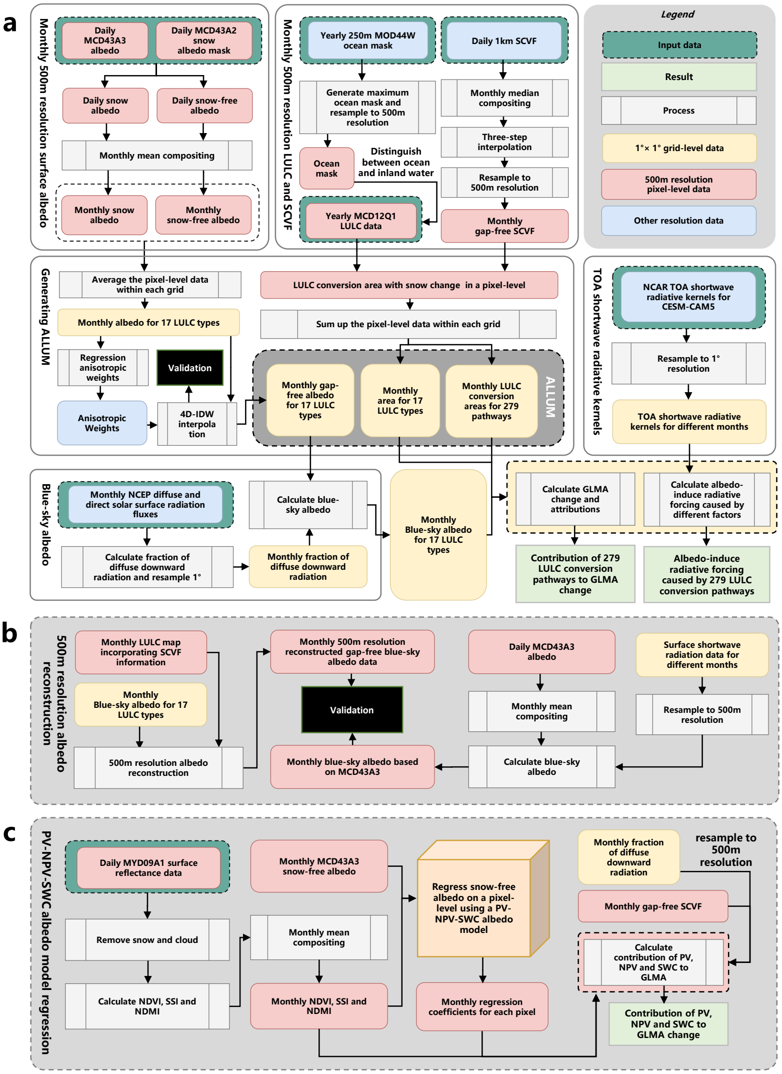

Supplementary Fig. S1 | **Damaged building samples in a Syrian conflict city on 0.5m- and 10m-resolution satellite images, respectively.**

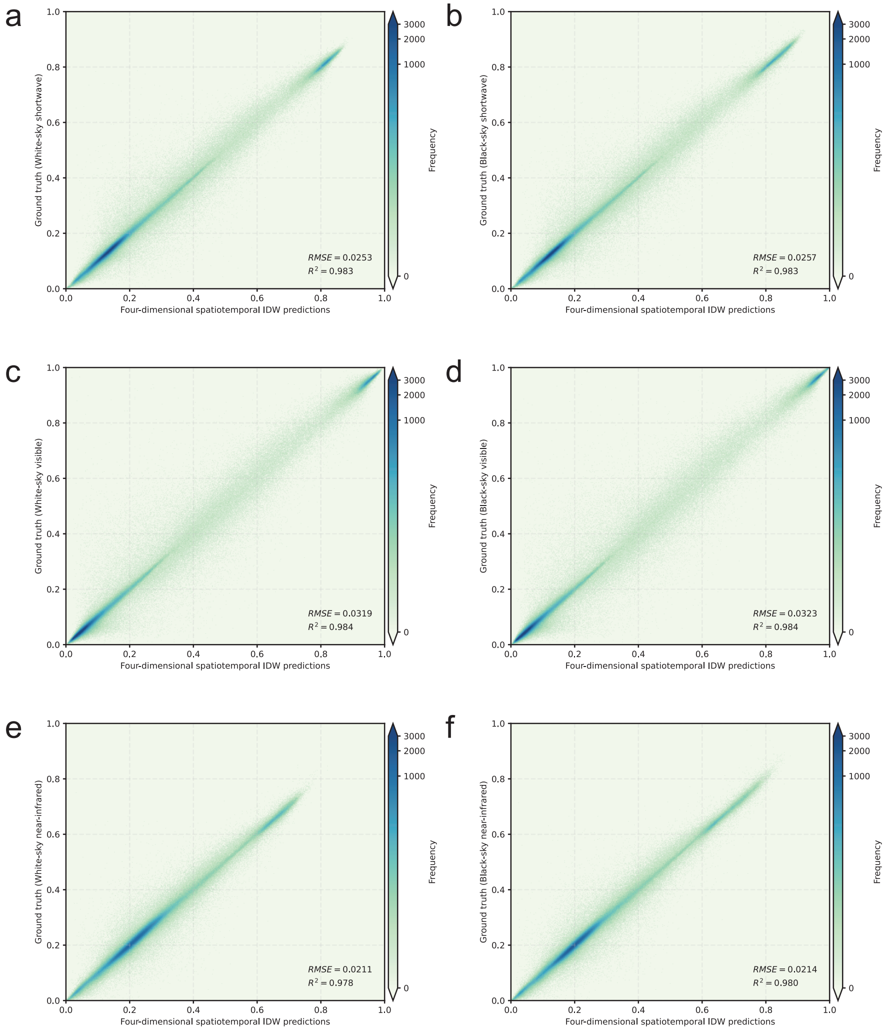

Supplementary Fig. S2 | The framework of our methodology. a, Generation of ALLUM, and contributions of LULC change to global land surface mean albedo (GLMA) change and the induced radiative forcing. **b,** Validations for reconstructing 500m-resolution blue-sky albedo. **c,** Contributions of changes in photosynthetic vegetation (PV), non-photosynthetic vegetation (NPV) and surface water content (SWC) to albedo change over regions without LULC conversions. The data in pink boxes and yellow boxes separately represent 500m-resolution pixel-level data and grid-level data.

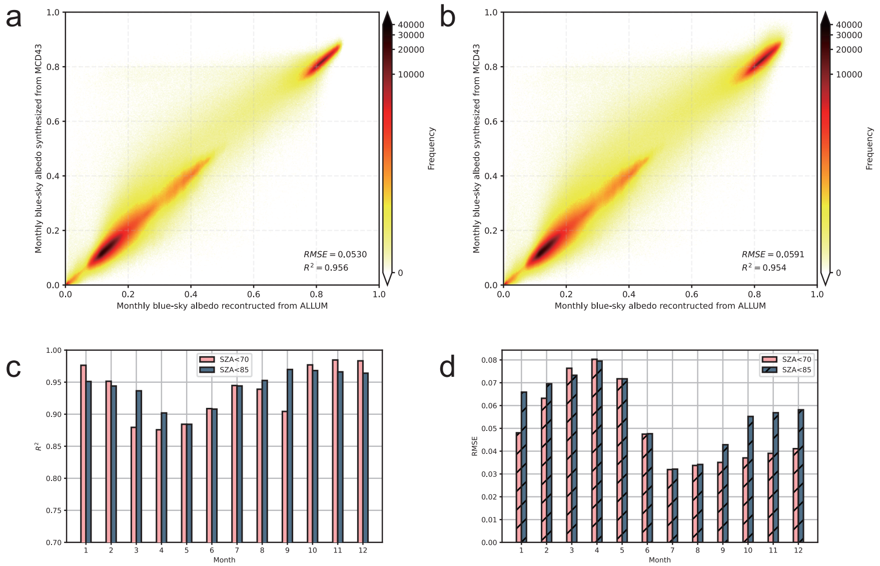

Supplementary Fig. S3 | Validations of the four-dimensional spatiotemporal Inverse Distance Weighted (IDW) interpolation. a, White-sky shortwave albedo. **b,** Black-sky shortwave albedo. **c,** White-sky vis albedo. **d,** Black-sky vis albedo. **e,** White-sky near-infrared albedo. **f,** Black-sky near-infrared albedo.

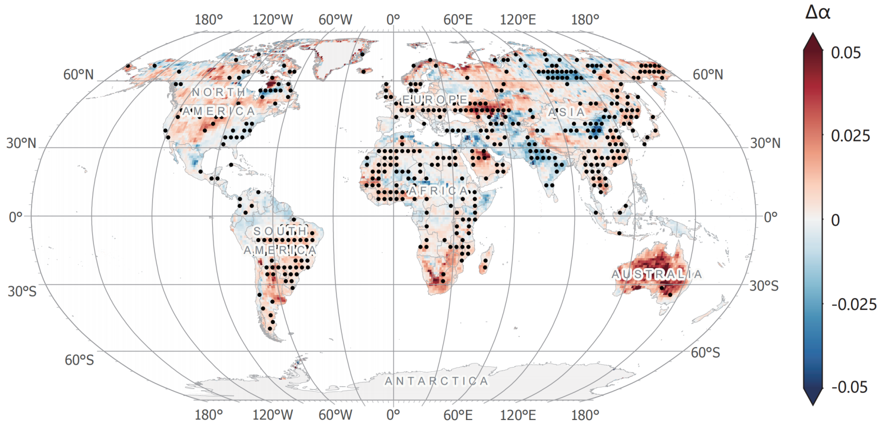

Supplementary Fig. S4 | Spatial distribution of albedo absolute changes in snow-free regions between 2001 and 2020 using albedo data in ALLUM. Black dots indicate bins with average albedo change between two independent temporal windows (2011-2020 and 2001-2010) that are statistically different from zero (two-sided Student's t-test; P-value leq 0.05).

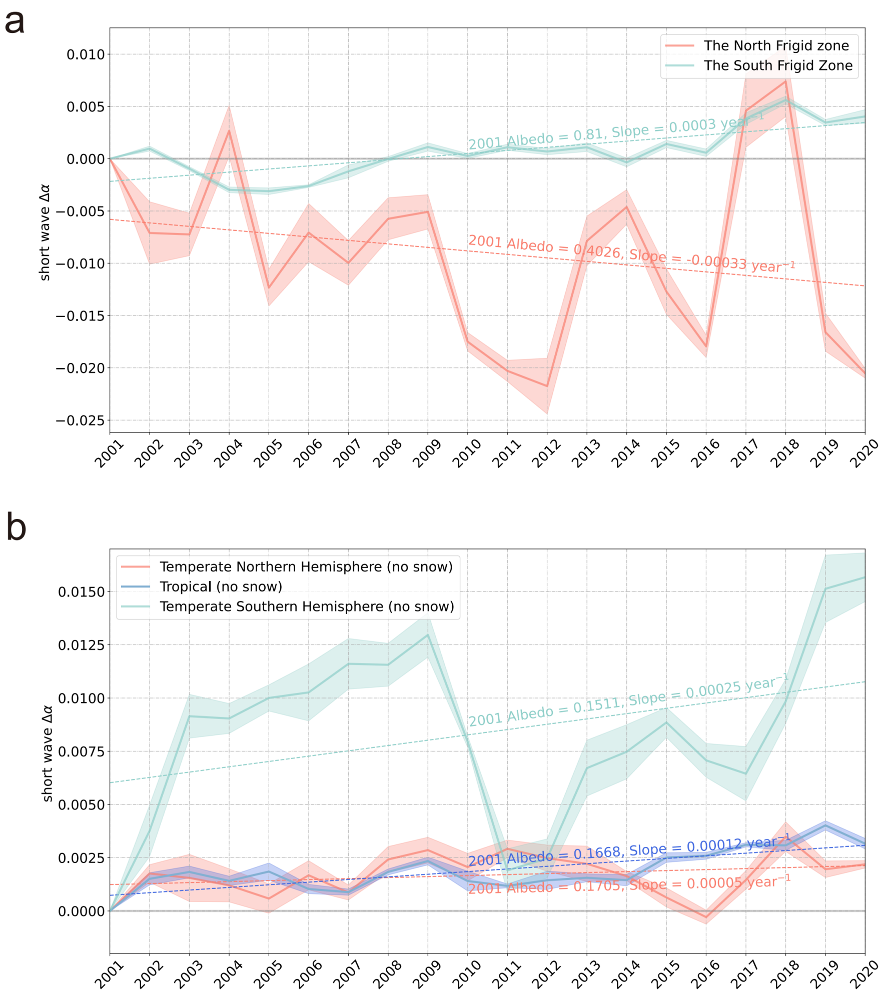

Supplementary Fig. S5 | The albedo changes over different regions. a, The changes in the north frigid zone (90°N-66°N) and the south frigid zone (66°S-90°S). **b,** The changes in the north temperate zone (66°N-23°N), tropical zone (23°N-23°S) and south temperate zone (23°S-66°S). The shaded areas denote the seasonal variations of albedo changes with one standard deviation.

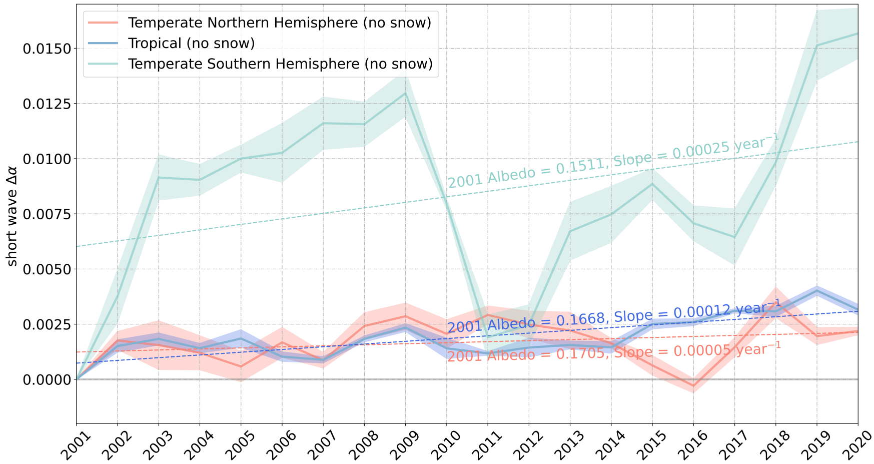

Supplementary Fig. S6 | The albedo changes of snow-free regions in the northern temperate zone (66°N-23°N), tropical zone (23°N-23°S) and southern temperate zone (23°S-66°S). The shaded areas denote the seasonal variations of albedo changes with one standard deviation.

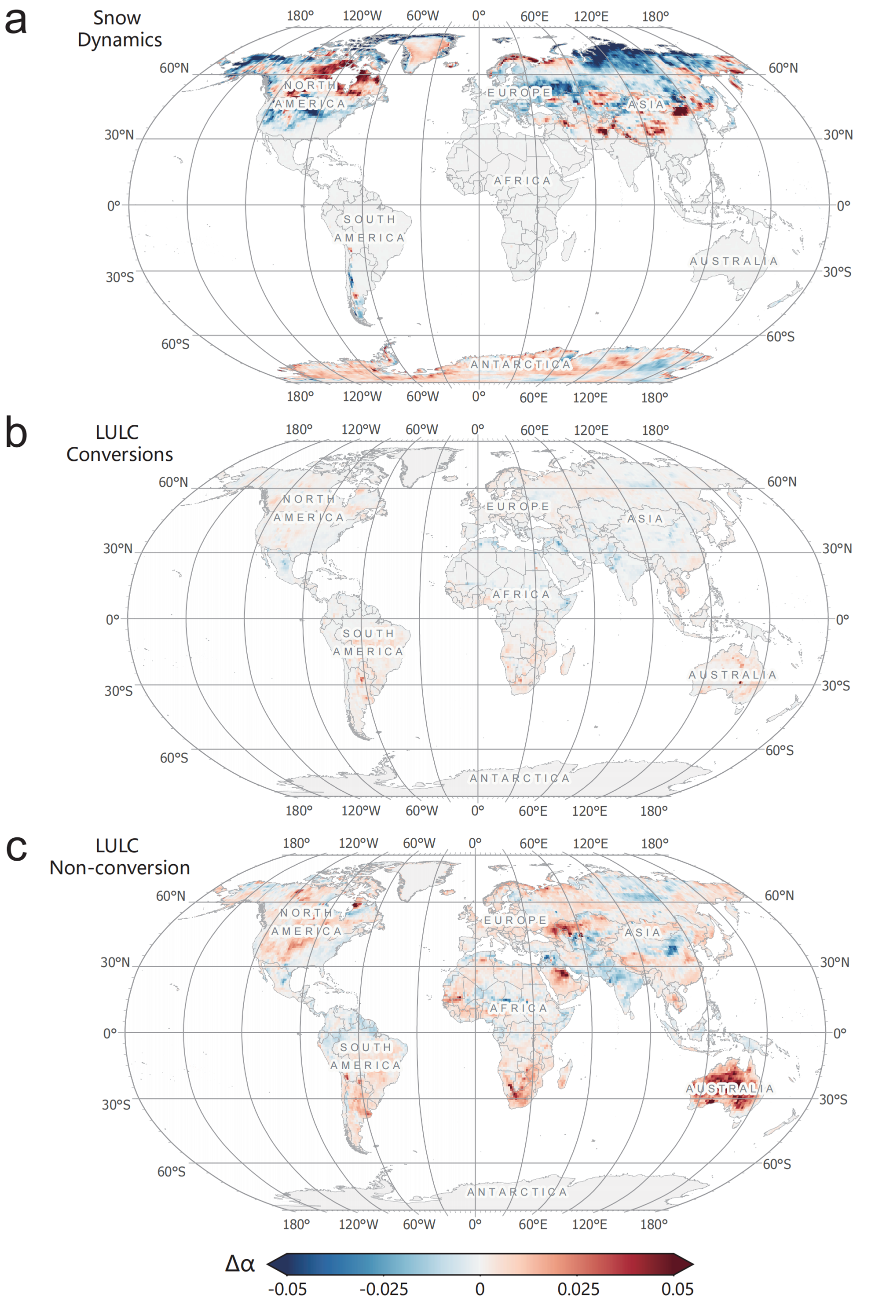

Supplementary Fig. S7 | Contributions to the land surface albedo changes from snow dynamics (a), LULC conversions (b) and albedo change in LULC non-conversion regions (c) during 2001-2020.

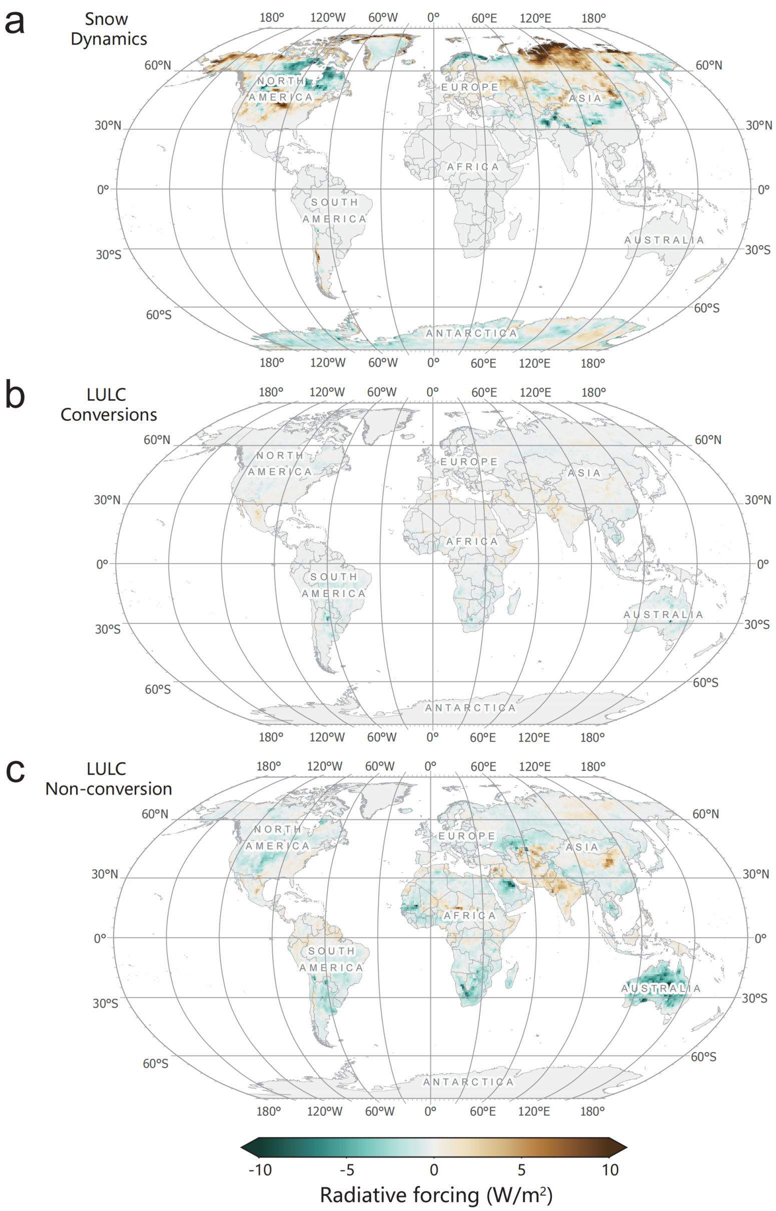

Supplementary Fig. S8 | Albedo-induced radiative forcing due to snow dynamics (a), LULC conversions (b), and albedo change in LULC non-conversion regions (c) during 2001-2020.

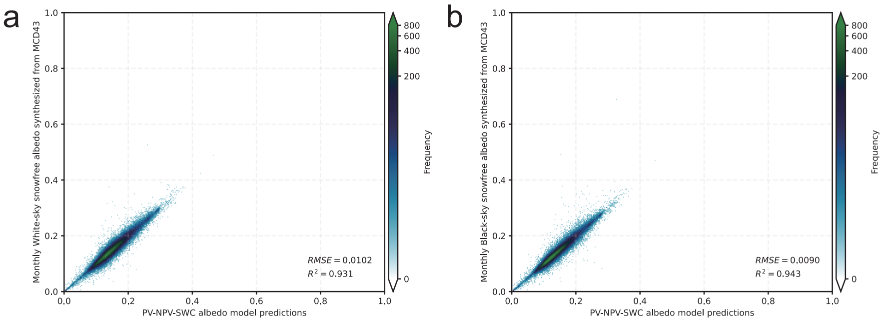

Supplementary Fig. S9 | Validations of the PV-NPV-SWC model regression. a, white-sky shortwave albedo. **b,** Black-sky shortwave albedo.

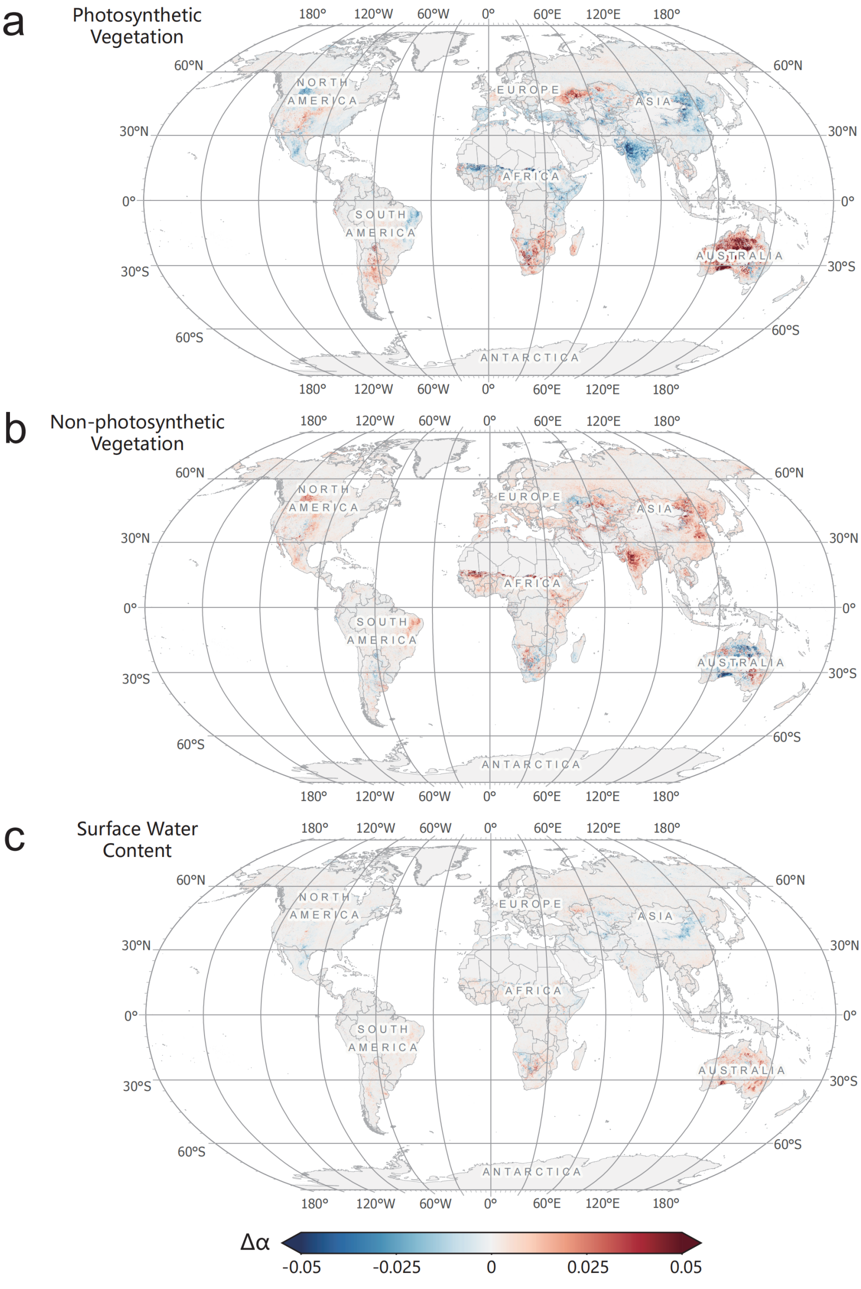

Supplementary Fig. S10 | Effects of the changes in photosynthetic vegetation (a), non-photosynthetic vegetation (b) and surface water content (c) on land surface albedo in LULC non-conversion regions during 2001-2020.

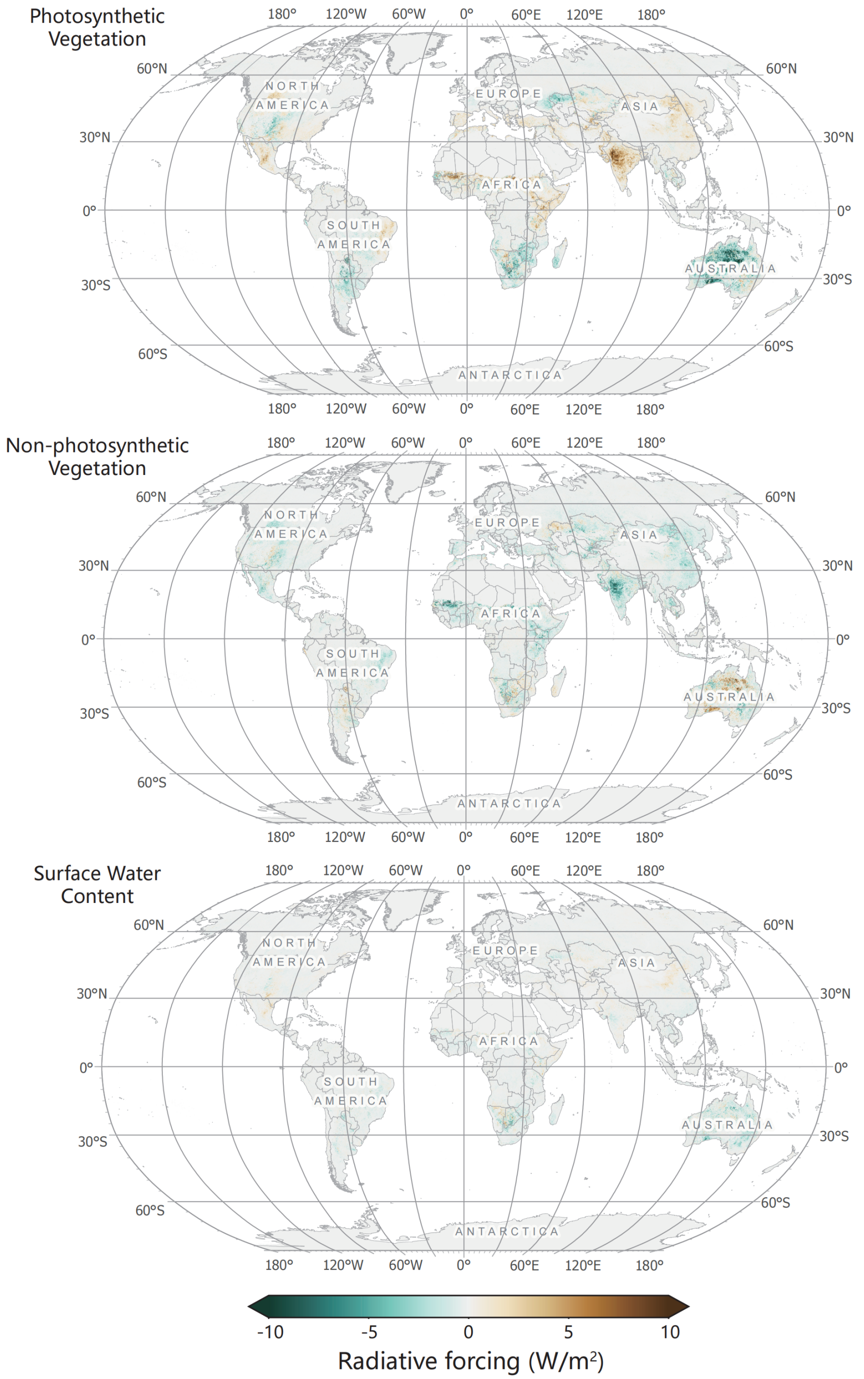

Supplementary Fig. S11 | Albedo-induced radiative forcing due to changes in photosynthetic vegetation (a), non-photosynthetic vegetation (b) and surface water content (c) in LULC non-conversion regions during 2001-2020.

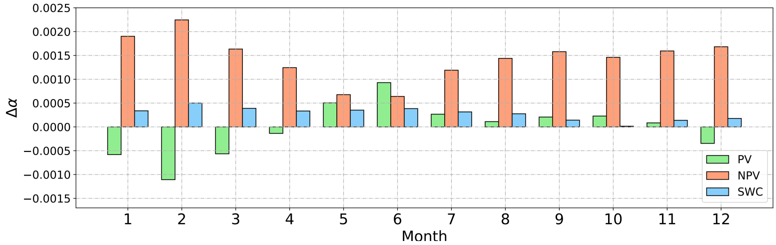

Supplementary Fig. S12 | The contributions of PV, NPV, and SWC to the monthly global land surface mean albedo change from 2001 to 2020. The albedo in the regions where the solar zenith angle is larger than 70° is filled with the mean in other months. Some regions worldwide with high normalized difference vegetation index (NDVI) cover vegetation such as evergreen forests in winter, which lead to the decrease of albedo. There is hardly green vegetation in winter in most of the regions, contributing little to albedo changes. We observe that the contribution is negative in winter. In summer, vegetation cover decreased in many regions with low NDVI values in the past 20 years, and the albedo change in these regions is sensitive to the change of NDVI. The decrease of green vegetation substantially increases albedo, which generally exceeds the decrease of albedo in regions with high NDVI values, so the contribution is positive in summer.

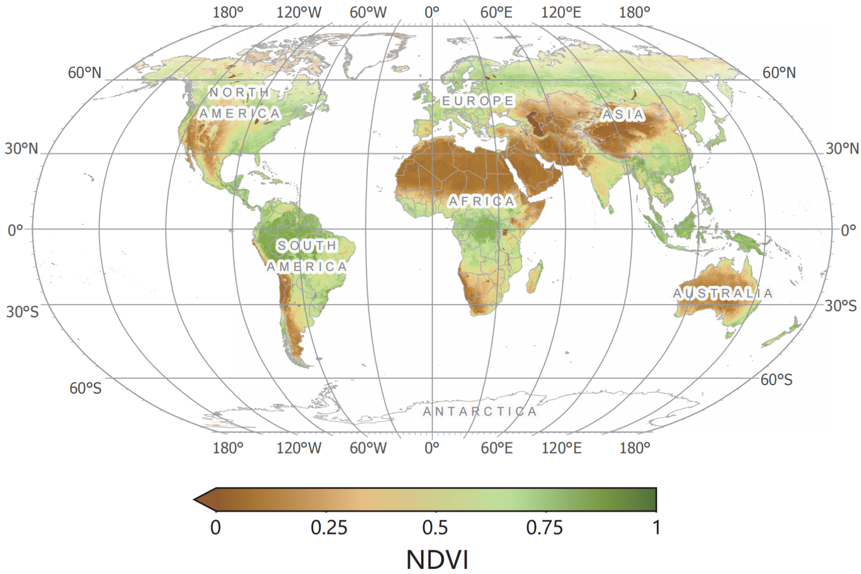

137
138 **Supplementary Fig. S13 | The global average NDVI for the year 2020.**

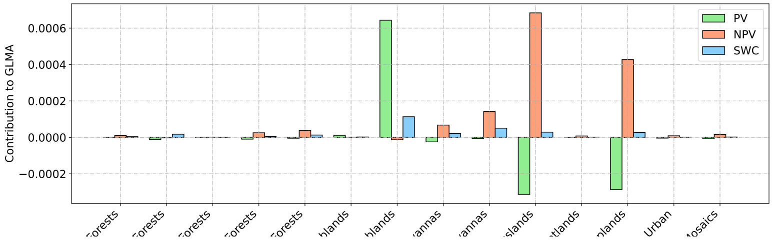

Supplementary Fig. S14 | Contributions of PV, NPV and SWC to GLMA over the LULC non-conversion regions.

3 Supplementary Tables

Supplementary Table S1 | The 16 land cover classes defined by IGBP. We have excluded Permanent Snow and Ice (15). The classes are from the MODIS/Terra+Aqua Land Cover Dataset, with class number in parentheses next to the class name [7].

Name	Acronym	Description
	Natural Vegetation	
Evergreen Needleleaf Forests (1)	ENF	Lands dominated by woody vegetation with a percent cover >60% and height exceeding 2 meters. Almost all trees remain green all year. Canopy is never without green foliage.
Evergreen Broadleaf Forests (2)	EBF	Lands dominated by woody vegetation with a percent cover >60% and height exceeding 2 meters. Almost all trees and shrubs remain green year-round. Canopy is never without green foliage.
Deciduous Needleleaf Forests (3)	DNF	Lands dominated by woody vegetation with a percent cover >60% and height exceeding 2 meters. Consists of seasonal needleleaf tree communities with an annual cycle of leaf-on and leaf-off periods.
Deciduous Broadleaf Forests (4)	DBF	Lands dominated by woody vegetation with a percent cover >60% and height exceeding 2 meters. Consists of broadleaf tree communities with an annual cycle of leaf-on and leaf-off periods.
Mixed Forests (5)	MF	Lands dominated by trees with a percent cover >60% and height exceeding 2 meters. Consists of tree communities with interspersed mixtures or mosaics of the other four forest types. None of the forest types exceeds 60% of landscape.
Closed Shrublands (6)	CSH	Lands with woody vegetation less than 2 meters tall and with shrub canopy cover >60%. The shrub foliage can be either evergreen or deciduous.
Open Shrublands (7)	OSH	Lands with woody vegetation less than 2 meters tall and with shrub canopy cover between 10-60%. The shrub foliage can be either evergreen or deciduous.
Woody Savannas (8)	WSA	Lands with herbaceous and other understory systems, and with forest canopy cover between 30-60%. The forest cover height exceeds 2 meters.
Savannas (9)	SAV	Lands with herbaceous and other understory systems, and with forest canopy cover between 10-30%. The forest cover height exceeds 2 meters.
Grasslands (10)	GRA	Lands with herbaceous types of cover. Tree and shrub cover is less than 10%.
Permanent Wetlands (11)	WET	Lands with a permanent mixture of water and herbaceous or woody vegetation. The vegetation can be present in either salt, brackish, or fresh water.

Name	Acronym	Description
		Developed and Mosaic Lands
Croplands (12)	CRO	Lands covered with temporary crops followed by harvest and a bare soil period (e.g., single and multiple cropping systems). Note that perennial woody crops will be classified as the appropriate forest or shrub land cover type.
Urban and Built-up Lands (13)	URB	Land covered by buildings and other man-made structures.
Cropland/Natural Vegetation Mosaics (14)	CVM	Lands with a mosaic of croplands, forests, shrubland, and grasslands in which no one component comprises more than 60% of the landscape.
		Non-Vegetated Lands
Barren (16)	BSV	Lands with exposed soil, sand, rocks, or snow and never has more than 10% vegetated cover during any time of the year.
Water Bodies (17)	WAT	Oceans, seas, lakes, reservoirs, and rivers. Can be either fresh or salt-water bodies.

Supplementary Table S2 | The methods for calculating the normalized NDVI, the spectral shape index (SSI) and the normalized multi-band drought index (NDMI).

Index	Methods
NDVI	$NDVI = \frac{band2-band1}{band2+band1}$
SSI	$SSI = \frac{slope_{nir-r}-slope_{g-b}}{slope_{nir-r}+slope_{g-b}}$ $slope_{nir-r} = \frac{band2-band1}{WL_{band2}+WL_{band1}}$ $slope_{g-b} = \frac{band4-band3}{WL_{band4}+WL_{band3}}$
NDMI	$NDMI = \frac{band2-(band6-band7)}{band2+(band6-band7)}$

Notes. $band1-7$ represents the surface reflectance of the corresponding bands for MYD09A1 V6.1. WL_{band} denotes the center wavelength of the corresponding band. The center wavelengths for bands 1-4 are $645\mu m$, $858\mu m$, $469\mu m$, and $555\mu m$, respectively.

Supplementary Table S3 | The maping between the IGBP land cover classes and LUH land cover classes [2]

LULC types in the LUH dataset	LULC types defined by IGBP
Primary lands	Evergreen Needleleaf Forests Evergreen Broadleaf Forests Deciduous Needleleaf Forests Deciduous Broadleaf Forests Mixed Forests Barren
Pasture Secondary lands	Closed Shrublands Open Shrublands Woody Savannas Savannas Grasslands Barren
Water	Permanent Wetlands Water Bodies
Cropland	Croplands Cropland/Natural Vegetation Mosaicss
Urban	Urban and Built-up Lands

References

[1] IPCC, . Masson-Delmotte, V. *et al.* (eds) *Climate change 2021: The physical science basis. contribution of working group I to the sixth assessment report of the intergovernmental panel on climate change.* (eds Masson-Delmotte, V. *et al.*) (Cambridge University Press, Cambridge, UK and New York, NY, USA, 2021).

[2] Ghimire, B. *et al.* Global albedo change and radiative cooling from anthropogenic land cover change, 1700 to 2005 based on MODIS, land use harmonization, radiative kernels, and reanalysis **41** (24), 9087–9096 (2014) .

[3] Smith, C. J. *et al.* Effective radiative forcing and adjustments in CMIP6 models **20** (16), 9591–9618 (2020) .

[4] Lejeune, Q. *et al.* Biases in the albedo sensitivity to deforestation in CMIP5 models and their impacts on the associated historical radiative forcing **11** (4), 1209–1232 (2020) .

[5] Hurtt, G. C. *et al.* Harmonization of land-use scenarios for the period 1500–2100: 600 years of global gridded annual land-use transitions, wood harvest, and resulting secondary lands **109** (1), 117 (2011) .

[6] Feng, G. *et al.* Multiscale climatological albedo look-up maps derived from moderate resolution imaging spectroradiometer BRDF/albedo products **8**, 083532 (2014) .

[7] Loveland, T. R. & Belward, A. S. The igbp-dis global 1km land cover data set, discover: First results. *International Journal of Remote Sensing* **18** (15), 3289–3295 (1997) .